The Effect of a Localized Topographic Irregularity on the Flow of a Boundary Current along the Continental Margin

SHENN-YU CHAO[1] AND GERALD S. JANOWITZ

Department of Marine Science and Engineering, North Carolina State University, Raleigh 27650

(Manuscript received 5 July 1978, in final form 2 January 1979)

ABSTRACT

A model for the effect of a localized topographic irregularity on a barotropic sheared current flowing along a continental margin with shallow water to the left of the current is developed. The topographic irregularity is assumed to be small and smooth compared to the background water depth and the background bottom slope, respectively. It is shown that the amplitude of the disturbance depends on the volume of the irregularity and its location on the margin. For a certain class of velocity and topographic profiles a closed form solution is obtained. The results show that the current is deflected seaward downstream of the disturbance with the maximum deflection occurring one-fourth of a wavelength downstream of the irregularity. Closed eddies are formed in shallow water and sometimes in deep water. If the ratio of relative shear to the speed of the approaching current is large at the continental margin, a simple analytical solution is applicable. The model is applied to the Gulf Stream flowing off the Carolina Coast in the region north of Charleston, South Carolina, and the results of Gulf Stream deflection and wavelengths of the leewaves are in modest agreement with observations.

1. Introduction

Recent satellite imagery (Legeckis (1978)) has shown that short waves and eddies on the length scale of 100–200 km frequently occur over the continental shelf and slope off the Carolina coast north of Charleston, South Carolina. Most of the published work which might explain these phenomena deals with the barotropic and baroclinic instabilities of a sheared current flowing over a sloping bottom in a rotating coordinate system. It is generally found that short shelf waves are more unstable than long shelf waves. Niiler and Mysak (1971) used a triangular current profile and a step-like bottom topography and found that barotropic shelf waves were most unstable for wavelengths on the order of 150 km and periods on the order of 10 days. Orlanski (1969) studied the influence of bottom slope on the baroclinic instability of the Gulf Stream using a two-layer model and found that south of Cape Romain, the maximum growth rate of unstable waves occurred at a wavelength of 220 km and a period of 10 days. While instabilities may well be the explanation for the existence of these short waves and small eddies, it is also possible that a topographic ridge off Charleston, known as the "Charleston bump", may be responsible for them. Fig. 1 shows the bathymetric map off the Carolina coast along with the location of the Charleston bump.

While analytical work on the steady flow over a topography in a rotating fluid has been extensive (e.g., Vaziri and Boyer, 1971; Hogg, 1973; McCartney, 1975; Janowitz, 1975; Johnson, 1978), most of them are concerned with upstream flows which are horizontally unsheared. Cottrell (1971) showed that the inclusion of a small upstream shear could affect flow patterns significantly. In this paper, we present a model for the barotropic flow of a horizontally sheared current flowing over a bump superimposed on a sloping bottom topography in a rotating fluid. While the current work was inspired by the observed seaward deflection of the Gulf Stream north of the Charleston bump, the results may be more applicable to other boundary currents flowing over a continental margin which varies little in the longshore direction except at isolated bumps. In Section 2a we give the general formulation of the problem leading to a linearized vorticity equation, and in Section 2b we present the general solution of the problem by applying a Fourier transform in the longshore direction and using a Green's function technique in the cross-shelf direction. In Section 2c we consider a special class of topography and sheared current profiles which yield an explicit solution. In Section 2d an approximate solution for the disturbance streamfunction by placing a rigid-wall boundary condition at the outer edge of the continental rise is given. It will be seen that this approximation is good if $V'_x L/V'$ is large at the continental rise, where V' is the undisturbed sheared

[1] Present affiliation: Research and Data Systems, Inc., Lanham, MD 20801.

0022-3670/79/050900-11$06.75

current, x' the cross-shelf distance from the coast and L the width of the shelf zone. Numerical results and the resultant streamline patterns are presented and discussed in Section 3. In Section 4 we summarize and discuss the possible applications as well as the shortcomings of this approach.

2. Analysis

a. Formulation

We consider a homogeneous fluid flowing steadily northward, with undisturbed upstream sheared current $V'(x')$ in the positive y' direction, where x' is the coordinate in the offshore direction; the origin is placed at the coast with y' axis corresponding to the shoreline. The current flows over a bottom depth $h_T'(x',y') = h'(x') - \tilde{h}'(x',y')$ composed of a depth profile h' which does not vary in the longshore direction and a bump $\tilde{h}'$ of maximum height $\tilde{h}_M$ localized near $y' = 0$ and $x' = x_0'$. We let L be the width of the continental margin, h_0 be the depth of the flat bottom ocean interior beyond the edge of the shelf zone and f_0 be the constant Coriolis parameter (see Fig. 2 for the configuration). We apply the rigid-lid and hydrostatic approximations and, in the absence of dissipation and baroclinicity and upstream vertical shear, take the horizontal velocity to be independent of the depth. We then nondimensionalize the horizontal velocities by f_0L, the reduced pressure $(p' - \rho_0 g z')$ by $\rho_0 f_0 L^2$, the horizontal coordinates by L, the total depth by h_0, and the bump topography by $\tilde{h}_M$. The governing equations are then

$$\left.\begin{aligned} uu_x + vu_y - v &= -p_x \\ uv_x + vv_y + u &= -p_y \\ (h_T u)_x + (h_T v)_y &= 0 \end{aligned}\right\}, \tag{1}$$

where (u,v) and p are dimensionless (x,y) velocities and pressure, respectively, and $h_T = h(x) - \epsilon\tilde{h}(x,y)$ is the dimensionless total depth function. We shall require that $\epsilon \equiv \tilde{h}_M/h_0$ is small compared to 1 so that the bump causes a disturbance of order ϵ to the basic flow $V(x)$. From the continuity equation in (1), a volume transport streamfunction ψ_T can be defined such that $-\psi_{Tx} = h_T v$, $\psi_{Ty} = h_T u$. The conservation of potential vorticity can be written as

$$h_T^{-1}(\zeta_T + 1) = F(\psi_T), \tag{2}$$

where

$$\zeta_T = -\nabla\cdot\left(\frac{1}{h_T}\nabla\psi_T\right) \tag{3}$$

is the relative vorticity of the local water column. Eq. (2) is not tractable for the problem we consider unless we make the following two approximations:

$$|\epsilon\tilde{h}| \ll |h|, \quad |\epsilon\nabla\tilde{h}| \ll |h_x|, \tag{4}$$

$$F(\psi_T) \approx F(\psi_0) + F'(\psi_0)\epsilon\psi \quad \text{for} \quad \psi_T = \psi_0 + \epsilon\psi, \tag{5}$$

where in (4) we require that the topographic irregularity be small and smooth, and in (5) that the ψ_0 is associated with the upstream sheared current $V(x)$, while ψ is the perturbed streamfunction generated by the bump. One notices that in making these approximations, as long as $|\epsilon\psi| \ll 1$, Eq. (5) is expected to be valid. The error in truncating the Taylor series expansion after two terms is of order

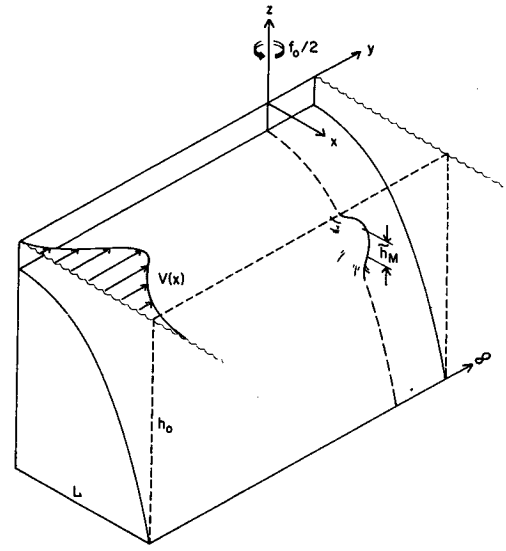

FIG. 2. Geometry of the flow field.

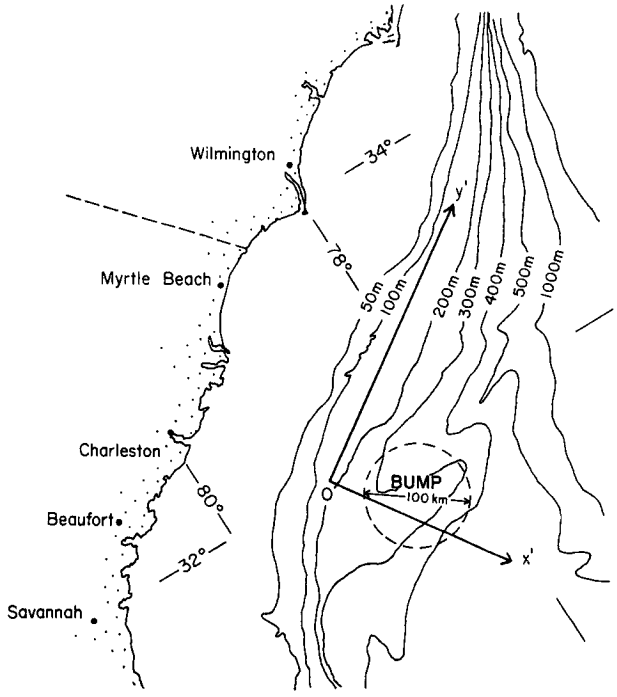

FIG. 1. The bathymetric map off the Carolina Coast, along with the location of the "Charleston bump".

$F''(\psi_0)(\epsilon\psi)^2$ which vanishes if F is a linear function of ψ_0. However, this argument will have to be justified *a posteriori*. We also notice that $|\epsilon\psi|$ does not have to be smaller than $|\psi_0|$ in Eq. (5). In the case that $|\psi_0| \ll 1$ in some region, $|\epsilon\psi|$ could be comparable or even larger than $|\psi_0|$ as long as the error involved in truncating the expansion remains small.

We also assume *a priori* that $\epsilon\psi$ vanishes far upstream ($y \to -\infty$), thus it follows from (2) that

$$F(\psi_0) = h^{-1}(1 + Vx) \equiv \Pi \tag{6}$$

is the upstream potential vorticity. From (6) we can determine that

$$F'(\psi_0) = -\frac{\Pi_x}{hV}. \tag{7}$$

Substitution of Eqs. (3)–(7) into (2) and neglecting terms of order ϵ^2 and higher, we then obtain the governing equation for the perturbed streamfunction ψ:

$$\nabla^2\psi - H\psi_x - (h\Pi_x/V)\psi = (1 + 2V_x - HV)\tilde{h} + V\tilde{h}_x. \tag{8}$$

For a typical boundary current such as the Gulf Stream, $V(x = 0) = V(x \to \infty) = 0$. We therefore require that boundary conditions for (8) be

$$\psi(x, -\infty) = \psi(\infty,y) = \psi(0,y) = 0, \tag{9}$$

i.e., the disturbance decays far upstream, far away from the coast, and there is no normal mass flux across the impermeable coast ($x = 0$). It should be remembered however, that the boundary conditions (9) must be complemented by a radiation condition as $y \to \infty$ to make the problem well posed.

b. Solution by a Green's function technique

To solve Eq. (8), we first define Fourier transforms of $\psi(x,y)$ and $\tilde{h}(x,y)$ as

$$\left.\begin{aligned} \phi(x,k) &= \frac{1}{\sqrt{2\pi}}\int_{-\infty}^{+\infty}\psi(x,y)e^{iky}dy \\ S(x,k) &= \frac{1}{\sqrt{2\pi}}\int_{-\infty}^{+\infty}\tilde{h}(x,y)e^{iky}dy \end{aligned}\right\}. \tag{10}$$

We can readily show that

$$\phi_{xx} - H\phi_x - \left(k^2 + \frac{h\Pi_x}{V}\right)\phi = (1 + 2V_x - VH)S + VS_x. \tag{11}$$

The Green's function solution for (11) is of the form

$$\phi(x,k) = \int_0^\infty G(x,\zeta;k)R(\zeta)d\zeta, \tag{12}$$

where $R(\zeta)$ is the right-hand side of (11) and

$$G(x,\zeta;k) = \begin{cases} \dfrac{\phi_1(x,k)\phi_2(\zeta,k)}{h(\zeta)D(k)}, & x < \zeta \\ \dfrac{\phi_1(\zeta,k)\phi_2(x,k)}{h(\zeta)D(k)}, & x > \zeta \end{cases} \tag{13}$$

where $\phi_1(x,k)$ and $\phi_2(x,k)$ are the homogeneous solutions of equation (11) satisfying the boundary conditions

$$\phi_1(0,k) = \phi_2(\infty,k) = 0 \tag{14}$$

and where

$$h(x)D(k) \equiv \phi_1\phi_{2x} - \phi_2\phi_{1x} \tag{15}$$

is the Wronskian of Eq. (11). The solution of (9) can then be expressed as

$$\psi(x,y) = \frac{1}{\sqrt{2\pi}}\int_{-\infty}^{+\infty}dke^{-iky}\int_0^\infty G(x,\zeta;k)R(\zeta)d\zeta. \tag{16}$$

The solution of (16) for large y is dominated by the worst singularity of the integrand nearest to the real axis of k. It can be shown by a residue calculation that a real and simple zero of $D(k)$ gives rise to a wavelike solution e^{-ik_0y}. Apart from zeal zeroes, there are possibly some imaginary zeroes of $D(k)$ and branch cuts in the complex k-plane, which gives rise to solutions decaying in y. The solution of (16) of course, depends, on the specific topography and sheared flow chosen, but a simple expression for the wavelike part of the solution can be obtained by a residue calculation.

If we suppose k_0 is a real simple zero of $D(k)$, then the Wronskian of (9) is zero and it follows that ϕ_1 is proportional to ϕ_2 at $k = k_0$ [$\phi_1 = C_0\phi_2$, where $C_0(k_0)$ is independent of x]. Assuming that the wavelike solution due to k_0 is a downstream wave, it can be shown by the residue theorem that wavelike solution is then

$$\psi_w = -\sqrt{2\pi}C_0^{-1}i \times \left[\int_0^\infty \frac{\phi_1(\zeta,k_0)}{h(\zeta)D'(k_0)}R(\zeta)d\zeta\right]\phi_1(x,k_0)e^{-ik_0y}, \tag{17}$$

where $D'(k_0) = dD/dk\big|_{k=k_0}$. Since $\phi_1(x,k_0)$ satisfies both boundary conditions at $x = 0$ and ∞, ψ_w is a zero-frequency continental shelf wave trapped over the shelf and slope region. Eq. (17) can be further simplified if we consider a delta-function bump, i.e., keep the volume of the bump fixed but shrink the size of the bump to zero. We then have

$$\left.\begin{aligned} \tilde{h}(x,y) &= V_b\delta(x - x_0)\delta(y) \\ S(x,k) &= \frac{V_b}{\sqrt{2\pi}}\delta(x - x_0) \end{aligned}\right\}, \tag{18}$$

where V_b is the volume of the bump divided by $\tilde{h}_M L^2$. Thus the wavelike part of the streamfunction

TABLE 1. Typical current parameters for which the $h\Pi_x/V$ and H are constant over the shelf and slope region. All the quantities are nondimensionalized by f_0^{-1} (time), L (horizontal length scale) and h_0 (height).

Case no.	$b = \frac{1}{2}hx/h$	θ	C	Mass transport $\psi_0(\infty)$	α	V_{max}	X_{max}
1	0.5	1.402	25.714	0.035	40.133	0.092	0.6
2	0.5	0.901	19.002	0.058	22.370	0.143	0.6
3	0.5	1.034	16.436	0.083	5.8	0.159	0.7
4	0.5	1.307	15.844	0.106	3.029	0.115	0.8
5	0.75	1.351	24.447	0.050	62.696	0.160	0.6
6	0.75	1.000	19.512	0.075	23.515	0.220	0.6
7	1.0	1.162	21.924	0.074	66.662	0.272	0.6
8	1.0	1.300	23.897	0.064	277.701	0.242	0.6
9	1.0	1.293	22.318	0.074	27.444	0.265	0.7
10	1.0	1.094	21.134	0.079	58.837	0.289	0.6

can be reduced to

$$\psi_w = -V_b C_0^{-1} i \frac{1}{D'(k_0)} \times [\Pi\phi_1 - V\phi_{1x}/h]_{\substack{x=x_0 \\ k=k_0}} \phi_1(x,k_0) e^{-ik_0 y}. \quad (19)$$

Eq. (19) is a useful formula from which we can compute the amplitude of the wavelike responses only if the shelf and slope topography and sheared current profile are specified. We further note from Eq. (11) that if k_0 is a singularity, then $-k_0$ is also a singularity and the results add to yield a real result.

c. Solution for constant coefficient profiles

Since H and $h\Pi_x/V$, in general, are functions of x, we cannot obtain explicit solutions. Therefore, we choose $h(x)$ and $V(x)$ which lead to an equation for ϕ with constant coefficients in x. We choose a topography of the form

$$h(x) = \begin{cases} e^{2b(x-1)}, & 0 \leq x \leq 1 \\ 1, & x \geq 1. \end{cases} \quad (20)$$

The sheared current profile over the shelf $[V_S(x)]$ is chosen in such a way that

$$\frac{h\Pi_x}{V} = -C, \quad (21)$$

where C is a positive constant. It follows from the definition of Π that $V_S(x)$ must satisfy

$$V_{Sxx} - HV_{Sx} + CV_S = H \equiv 2b, \; 0 \leq x \leq 1, \quad (22)$$

along with the additional constraints that the current vanishes at the coast $[V_S(0) = 0]$, there is no countercurrent $[V_S(x) \geq 0$ for all $x \geq 0]$, and that the sheared current is assumed to have only one maximum. It follows that

$$V_S(x) = HC^{-1}[1 + e^{bx} \sin(\sqrt{C - b^2}x - \theta)/\sin\theta], \quad (23)$$

where C and θ are two constants to be chosen, constrained by the conditions that $C > b^2$ (V_S is oscillatory for $0 \leq x \leq 1$), $V_{Sx}(0) > 0$, and $\sqrt{C - b^2} < 2\pi$ (V_S has only one maximum). Beyond the shelf and slope region, the sheared current $V_0(x)$ is defined by

$$V_0(x) = V_S(1)e^{-\alpha(x-1)}, \quad x \geq 1, \quad (24)$$

so that V is continuous across $x = 1$. The constant α is chosen to be equal to $-V_{Sx}(1)/V_S(1)$ so that V_x is continuous across $x = 1$; the continuity of V and V_x requires that ψ and ψ_x be continuous across $x = 1$. Typical current profiles for different exponential shelves are listed in Table 1 for reference.

With the topography and sheared current chosen, the governing equation (11) can be reduced to

$$\left.\begin{aligned} \phi_{xx} - H\phi_x + (C - k^2)\phi &= R(x), & 0 \leq x \leq 1 \\ \phi_{xx} - (\alpha^2 + k^2)\phi &= R(x), & x \geq 1 \end{aligned}\right\}. \quad (25)$$

Eq. (25) is a constant coefficient differential equation and thus has simple homogeneous solutions. The homogeneous solution $\phi_1(x,k)$ defined in (14) is

$$\phi_1(x,k) = \begin{cases} e^{bx} \sin\sqrt{\beta^2 - k^2}x, & x \leq 1 \\ a_- \exp[-(\alpha^2 + k^2)^{1/2}x] + a_+ \exp[(\alpha^2 + k^2)^{1/2}x], & x \geq 1 \end{cases} \quad (26)$$

where $\beta^2 = C - b^2$, and where a_- and a_+ are determined by matching ϕ_1 and ϕ_{1x} across $x = 1$:

$$a_\pm = \tfrac{1}{2} \exp[b \mp (\alpha^2 + k^2)^{1/2}] \left[\left(1 \pm \frac{b}{\sqrt{\alpha^2 + k^2}}\right) \sin\sqrt{\beta^2 - k^2} \pm \frac{\sqrt{\beta^2 - k^2}}{\sqrt{\alpha^2 + k^2}} \cos\sqrt{\beta^2 - k^2} \right]. \quad (27)$$

Similarly, ϕ_2 is

$$\phi_2(x,k) = \begin{cases} e^{bx}(b_- \sin\sqrt{\beta^2 - k^2}x + b_+ \cos\sqrt{\beta^2 - k^2}\,x), & x \leqslant 1 \\ \exp[-(\alpha^2 + k^2)^{1/2}x], & x \geqslant 1 \end{cases} \tag{28}$$

where

$$b_+ = \exp[-b - (\alpha^2 + k^2)^{1/2}]\left[\cos\sqrt{\beta^2 - k^2} + \frac{b + \sqrt{\alpha^2 + k^2}}{\sqrt{\beta^2 - k^2}} \sin\sqrt{\beta^2 - k^2}\right]$$

$$b_- = \exp[-b - (\alpha^2 + k^2)^{1/2}]\left[\sin\sqrt{\beta^2 - k^2} - \frac{b + \sqrt{\alpha^2 + k^2}}{\sqrt{\beta^2 - k^2}} \cos\sqrt{\beta^2 - k^2}\right]. \tag{29}$$

The Wronskian of Eq. (25) can be computed from (15), and it follows that

$$D(k) = -\exp[b - (\alpha^2 + k^2)^{1/2}][(\sqrt{\alpha^2 + k^2} + b) \sin\sqrt{\beta^2 - k^2} + \sqrt{\beta^2 - k^2} \cos\sqrt{\beta^2 - k^2}]. \tag{30}$$

Thus the eigenvalues (wavenumbers of the zero-frequency shelf waves) exist at $k = k_0$, where

$$\tan\sqrt{\beta^2 - k_0^2} = -\frac{\sqrt{\beta^2 - k_0^2}}{b + \sqrt{\alpha^2 + k_0^2}}. \tag{31}$$

The mass transport streamfunction can be found by substituting (26), (28) and (30) into (16). It is easily seen that the Green's function $G(x,\zeta; k)$ is an even function of $(\beta^2 - k^2)^{1/2}$. Therefore, branch cuts in the complex k-plane come only from $(\alpha^2 + k^2)^{1/2}$. We define two branch cuts on the imaginary axis of the k-plane from $i\alpha$ to $i\infty$, and from $-i\alpha$ to $-i\infty$ (see Fig. 3). It can also be shown that the real eigenvalues are shifted to the lower half of the complex k-plane if we include some friction in the formulation. The term e^{-iky} in the integrand of (16) requires that one should close the contour of integration on the lower half of the k-plane for a downstream solution ($y > 0$). Therefore, wavelike responses appear only downstream of the bump, justifying our *a priori* assumption that the disturbance decays far upstream. We also note that Eq. (31) has a pair of trivial eigenvalues $k_0 = \pm\beta$ for which the corresponding eigenfunctions are zero and have no contribution to $\psi(x,y)$. Apart from $\pm\beta$, numerical calculation suggests that there is only one pair of $\pm k_0$ which satisfy (31); these eigenvalues belong to the first-mode stationary shelf waves. Comparing to the result of Brooks (1978), who show that only second- and third-mode shelf waves can be stationary for the Cape Fear section, one may wonder if our model is realistic. However, the dispersion diagram is in general highly dependent on local waveguide characteristics, such as shelf slopes and sheared current profiles. Considering the fact that waveguide characteristics change rapidly from Cape Romain to Cape Hatteras, what applies at Cape Fear may not apply upstream of Charleston, which is at least 300 km from Cape Fear. Apart from the real eigenvalues $\pm k_0$, there are a number of imaginary eigenvalues k_j of (31), depending on the magnitude of α, which give rise to a decaying response.

It is sufficient for our purpose to consider only the delta-function bump. The actual flow pattern over a realistic bump can be found by integrating the delta-function solution over an extended topography. It is found for the isolated bump that

$$\psi(x,y) = \frac{-2V_b b_-}{D'(k_0)}\left[\Pi\phi_1 - \frac{V}{h}\phi_{1x}\right]_{\substack{x=x_0 \\ k=k_0}} \phi_1(x,k_0) \sin k_0 y$$

$$- iV_b \sum_j \left\{\frac{b_-}{D'(k_j)}\left[\Pi\phi_1 - \frac{V}{h}\phi_{1x}\right]_{x=x_0}\right\}_{k=-k_j} \phi_1(x,k_j) \exp(-|k_j|y) + I(x,y), \qquad y > 0, \tag{32}$$

$$\psi(x,y) = iV_b \sum_j \left\{\frac{b_-}{D'(k_j)}\left[\Pi\phi_1 - \frac{V}{h}\phi_{1x}\right]_{x=x_0}\right\}_{k=k_j} \phi_1(x,k_j) \exp(|k_j|y) + I(x,-y), \qquad y < 0, \tag{33}$$

where $k_0 > 0$, the k_j's are the positive imaginary eigenvalues, and

$$D'(k) = -\exp[b - (\alpha^2 + k^2)^{1/2}]\left[\left(\frac{k}{\sqrt{\alpha^2 + k^2}} + k\right) \sin\sqrt{\beta^2 - k^2} - \frac{k}{\sqrt{\beta^2 - k^2}}(1 + \sqrt{\alpha^2 + k^2} + b) \cos\sqrt{\beta^2 - k^2}\right] \tag{34}$$

and $I(x,y)$ is the integral of (16) around the branch cuts and can be expressed as

$$I(x,y) = \begin{cases} \dfrac{V_b}{\pi}\sqrt{\dfrac{h(x)}{h(x_0)}}\displaystyle\int_\alpha^\infty \dfrac{\{V(x_0)\sqrt{\beta^2+t^2}\cos(\sqrt{\beta^2+t^2}x_0) - [1+V_x(x_0) - bV(x_0)]\sin(\sqrt{\beta^2+t^2}x_0)\}}{(\sqrt{\beta^2+t^2}\cos\sqrt{\beta^2+t^2} + b\sin\sqrt{\beta^2+t^2})^2 + (t^2-\alpha^2)\sin^2\sqrt{\beta^2+t^2}} \\ \qquad \times \sqrt{t^2-\alpha^2}\sin(\sqrt{\beta^2+t^2}x)e^{-ty}dt, \qquad 0 \leqslant x \leqslant 1 \\ \dfrac{V_b}{\pi}\dfrac{1}{\sqrt{h(x_0)}}\displaystyle\int_\alpha^\infty \{\sin[\sqrt{t^2-\alpha^2}(1-x)](\sqrt{\beta^2+t^2}\cos\sqrt{\beta^2+t^2} - b\sin\sqrt{\beta^2+t^2}) \\ \quad - \sqrt{t^2-\alpha^2}\sin\sqrt{\beta^2+t^2}\cos[\sqrt{t^2-\alpha^2}(1-x)]\} \\ \quad \times \dfrac{\{[1+V_x(x_0) - bV(x_0)]\sin(\sqrt{\beta^2+t^2}x_0) - V(x_0)\sqrt{\beta^2+t^2}\cos(\sqrt{\beta^2+t^2}x_0)\}}{(\sqrt{\beta^2+t^2}\cos\sqrt{\beta^2+t^2} + b\sin\sqrt{\beta^2+t^2})^2 + (t^2-\alpha^2)\sin^2\sqrt{\beta^2+t^2}} e^{-ty}dt \; x \geqslant 1. \end{cases} \tag{35}$$

It is easily seen from (35) that $I(x,y) = I(x,-y)$. The decaying part of streamfunction is therefore an even function of y. Before turning to a numerical calculation of (32)–(35), we turn to a channel analogue of the current problem which be valid if $\alpha\ (\equiv |V_x/V|_{x=1})$ is large.

d. Channel flow analogue

For a laterally sheared stream well-contained in the shelf and slope region, the value of α is usually large. In those cases the solution can be approximated by that of a channel with the same topography and sheared current profiles but adding the impermeable sidewall boundary condition at $x = 1$. The boundary condition as $x \to \infty$ is then replaced by $\phi(x = 1) = 0$. In fact, it will be shown below that the channel flow analogue is exact in the limit of $\alpha \to \infty$. A similar approximation for long shelf waves without a mean current to separate the flow over the shelf from the flow beyond the shelf was found by Buchwald and Adams (1968) and proven to be a very useful approximation for the study of wave diffraction problems. Therefore the channel flow analogue to be discussed below could be very useful in the future if other kinds of inhomogeneities of the continental shelf waveguide are included.

We can understand this channel approximation as follows. Let us assume that α is large and that the bump is located at $x_0 < 1$. We first solve for ψ for $x \geqslant 1$, subject to $\psi(0,y) = \psi(1,y) = 0$ and Eq. (9). We call this solution ψ_{S0}. The solution over the flat bottom is of the form

$$\psi_{00} = \frac{1}{\sqrt{2\pi}} \times \int_{-\infty}^{+\infty} \exp[-(\alpha^2+k^2)^{1/2}(x-1) - iky]F(k,x)dk.$$

The function $F(k,x)$ is determined by requiring that $\psi_{00x}(1,y) = \psi_{S0x}(1,y)$ or that

$$\psi_{S0x}(1,y) = -\frac{1}{\sqrt{2\pi}}\int_{-\infty}^{+\infty}\sqrt{\alpha^2+k^2}F(k,x)e^{-iky}dk.$$

It is clear that $F(k,x) = O(1/\alpha)$ and hence $\psi_{00} = O(1/\alpha)$; this must be matched to (and forces) a correction to ψ_{S0}, say, ψ_{S1}. Hence, the correction to ψ_{S0} would be $O(1/\alpha)$ or smaller except for $|y| < 1/\alpha$. We now have determined the streamfunction continuous across $x = 1$ through order $1/\alpha$ and ψ_x continuous through order 1. We could then use ψ_{S1x} to determine ψ_{01} [$=O(1/\alpha^2)$] and so on. The original solution, ψ_{S0}, is then a reasonable representation for ψ for $x \leqslant 1$.

We now obtain the solution for the channel flow case, i.e., ψ_{S0}. Consider the equation

$$\psi_{xx} + \psi_{yy} - H\psi_x + C\psi = V_b[(1 + 2V_x - VH)\delta(x - x_0) + V\delta'(x - x_0)]\delta(y), \tag{36}$$

with the boundary conditions $\psi(0,y) = 0$ and

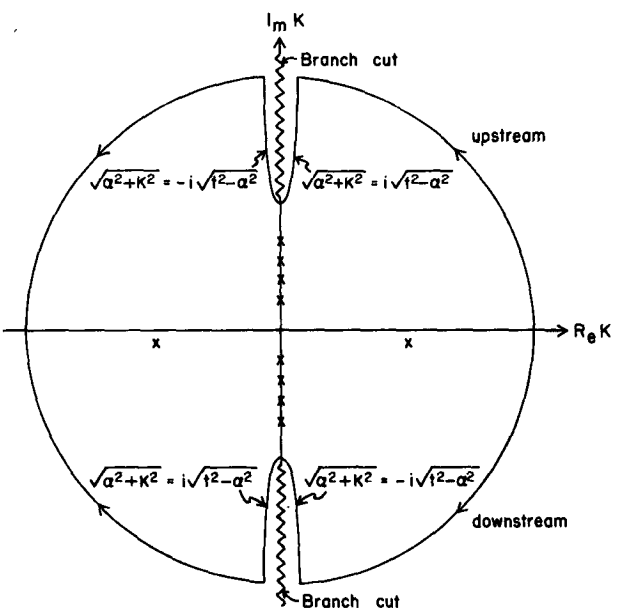

FIG. 3. Contours of integrations for the upstream and downstream in the complex k-plane, and the definition of the branch.

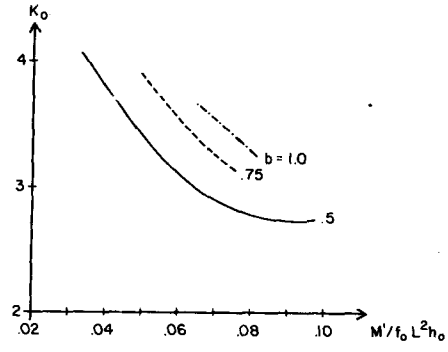

FIG. 4. Wavenumber of the lee wave (k) versus the total mass transport (M) for different values of b. All quantities are dimensionless.

$\psi(1,y) = 0$. The perturbation streamfunction ψ is then expanded as

$$\psi(x,y) = e^{bx} \sum_{n=1}^{\infty} A_n(y) \sin n\pi x. \tag{37}$$

Substitution of (37) into (36) leads, after application of the orthogonality property of $\sin n\pi x$, to

$$A_{nyy} + (\beta^2 - n^2\pi^2)A_n = \left\{2V_b \int_0^1 [(1 + 2V_x - VH)\delta(x - x_0) + V\delta'(x - x_0)]e^{-bx} \sin n\pi x\right\}\delta(y). \tag{38}$$

Therefore $A_n(y)$ satisfies the homogeneous part of equation (38) for all $|y| > 0$, together with the condition

$$A_{ny}(0^+) - A_{ny}(0^-) = 2V_b e^{-bx_0}\{[1 + V_x(x_0) - bV(x_0)] \sin n\pi x_0 - n\pi V(x_0) \cos n\pi x_0\}. \tag{39}$$

Eq. (39) is obtained by integrating (38) with respect to y from 0^- to 0^+.

As $\alpha \to \infty[V(1) = 0]$, one can easily show from (23) and associated constraints that $\pi \leqslant \beta \leqslant 2\pi$. Therefore, only the $n = 1$ component in (38) is a wavelike mode and modes higher than $n = 1$ are all decaying modes. Inclusion of some friction will place the wavelike mode downstream. It follows that the $n = 1$ mode is downstream solution, while all the higher modes exist both downstream and upstream. Since (38) is even in y, the decaying modes are therefore symmetric with respect to $y = 0$. We can also easily show that

$$\psi_1 = \frac{2V_b}{\sqrt{\beta^2 - \pi^2}}\{[1 + V_x(x_0) - bV(x_0)]e^{-bx_0} \sin \pi x_0 - \pi V(x_0)e^{-bx_0} \cos \pi x_0\}e^{bx} \sin \pi x \sin \sqrt{\beta^2 - \pi^2}\, y, \tag{40}$$

and for $n = 1$,

$$\psi_n = \frac{-V_b}{\sqrt{n^2\pi^2 - \beta^2}} e^{-bx_0}\{[1 + V_x(x_0) - bV(x_0)] \times \sin n\pi x_0 - n\pi V(x_0) \cos n\pi x_0\}e^{bx} \times \sin n\pi x \exp[-(n^2\pi^2 - \beta^2)^{1/2}|y|]. \tag{41}$$

The ψ_n's are defined such that for $y > 0$,

$$\psi = \psi_1 + \sum_{n=2}^{\infty} \psi_n$$

and for $y < 0$,

$$\psi = \sum_{n=2}^{\infty} \psi_n.$$

The proof of equivalence between the result of Section 2c (as $\alpha \to \infty$) and that of this section is immediate. Notice that from (31), $k_0^2 = \beta^2 - \pi^2$ (if $\alpha \to \infty$), and accordingly from (29) and (34)

$$\frac{b_-}{D'(k_0)} = -\frac{e^{-2b}}{\sqrt{\beta^2 - \pi^2}}, \quad \alpha \to \infty.$$

Therefore ψ_1 is equivalent to the downstream wavelike part of Eq. (32). For the decaying solutions, $k_j^2 = \beta^2 - n^2\pi^2$ (recall that k_j's are positive imaginary, and hence $k_j^2 < 0$), it also follows that

$$\frac{b_-}{D'(k_j)} = -\frac{e^{-2b}}{i\sqrt{n^2\pi^2 - \beta^2}}, \quad \alpha \to \infty.$$

Therefore, ψ_n in (41) is equivalent to the nth decaying solution in (32) and (33). The branch cuts disappear as $\alpha \to \infty$, as does the integral $I(x,y)$ in (32). Thus our proof of channel flow analogue is completed. For $\alpha > 10$, the streamline patterns obtained by using (40) and (41) are virtually identical to the exact result.

3. Numerical results

The analysis of horizontally sheared flow over a bump on a sloping topography in the last section was based on a specific class of sheared current and topographic profiles. However, some interesting qualitative conclusions can still be extracted from it. Our objective is to explore the qualitative behavior when the Gulf Stream flows over the Charleston bump. Therefore, the profiles listed in Table 1 constitute only a narrow range of the complete spectrum of the constant coefficient profiles, those which have the same order of magnitude of shelf slopes and total mass transports of the Gulf Stream off the Charleston bump.

Fig. 4 shows the dimensionless wavenumber of the lee wave versus the total mass transport for different values of b. The position where V is a maximum is fixed at $x_{max} = 0.6$ so that the shape of the sheared current profiles for the same b are similar. The wavenumbers are determined by the transcendental relation (31). It turns out that the wavenumber increases with increasing b or decreas-

ing mass transport M. For an unsheared barotropic flow of speed U over a bottom sloping downward to the right with angle θ_0, we would expect the wavenumber to be proportional to $(\theta_0/U)^{1/2}$. In our case b is a measure of θ_0, while M is a measure of U, so that $k_0 \approx (b/M)^{1/2}$, which is in agreement with Fig. 4. Physically, a larger mass transport tends to sweep the disturbance downstream faster and thus elongate the wavelength, while a steeper bottom slope acts as a stronger restoring force and thus shortens the wavelength. We also notice that if $L = 100$ km and $h_0 = 1$ km, then $f_0L^2h_0 = 1000$ Sv. Thus $M'/f_0L^2h_0 = 0.05$ corresponds to a volume flux of 50 Sv.

If the bottom topography and sheared current profile are specified, the amplitude of the lee wave can be easily computed from (32). Figs. 5a–5c show the amplitude of the lee wave versus the position of the delta function bump, together with the $V(x)$ profile for three cases in Table 1 (cases 2, 4 and 7, respectively). The amplitude A of the lee wave is defined such that wavelike part of the solution is

$$\tilde{\psi}_w = \epsilon\psi_w = A\epsilon V_b\phi_1(x,k_0)\sin k_0 y.$$

The channel analogue has

$$A = \frac{2}{\sqrt{\beta^2 - \pi^2}}[(1 + V_x - bV)e^{-bx_0} \times \sin\pi x_0 - \pi V(x_0)\cos\pi x_0].$$

It can be seen from Fig. 5 that the location of the bump where it generates the maximum amplitude of the lee wave occurs to the onshore side of the position of maximum $V(x)$, and the maximum lee wave amplitude and location of the maximum amplitude vary only slightly with velocity profile.

There are essentially two reasons which prohibit us from considering realistic topographic features off the Carolina coast in detail. First, the shelf narrows gradually northward from Charleston to Cape Hatteras, which differs from the uniform longshore shelf with an isolated topographic irregularity that we consider here. Second, the cross-shelf topographic profile in the vicinity of Charleston is not an exponential shelf. However, an exponential shelf of the Buchwald-Adams type does give us relatively simple analytical solutions which, conceivably, will shed some light on similar problems with a different cross-shelf topography. As a first example, we choose $b = 0.5$, $\theta = 0.9$, $C = 19.0$, corresponding to case 2 in Table 1. The dimensionless mass transport corresponds to a dimensional value of 58 Sv if we take $f_0 = 0.8 \times 10^{-4}$ s^{-1}, $L = 125$ km, $h_0 = 1$ km. The velocity maximum (V_{max}) is then 143 cm s^{-1}. We also choose the dimensionless volume of the bump (ϵV_b) to be 0.03 and place the singularity at $x_0 = 0.5$. The resulting streamline pattern is shown in Fig. 6a. The stream

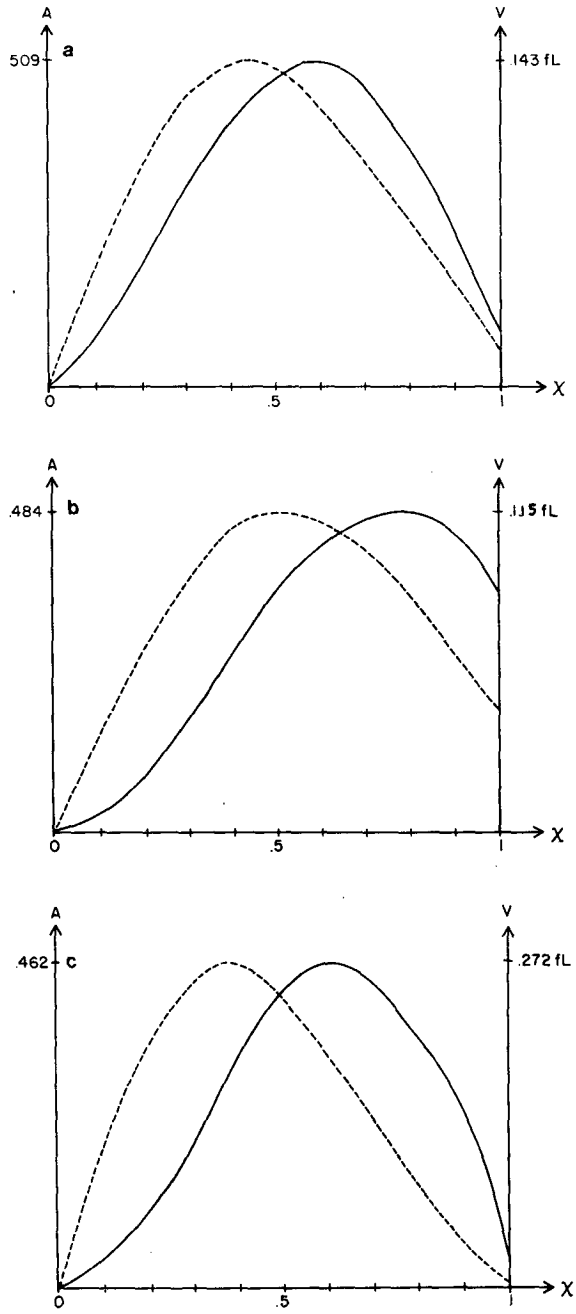

FIG. 5. The sheared current profile $V(x)$ over the shelf and slope region (solid line), and the amplitude A of the lee wave as a function of the position of the delta function bump (x) (dashed line) for (a) case 2, (b) case 4 and (c) case 7 of Table 1.

is deflected approximately 60 km from the coast, 40 km north of the singularity. The wavelength (λ) of the lee wave is approximately 165 km. Eddies exist near the coast centered at distances of approximately $40 + n\lambda$ km ($n = 0, 1, 2 \ldots$) downstream of the singularity. Weak eddies on the seaward side of the stream also exist. Large de-

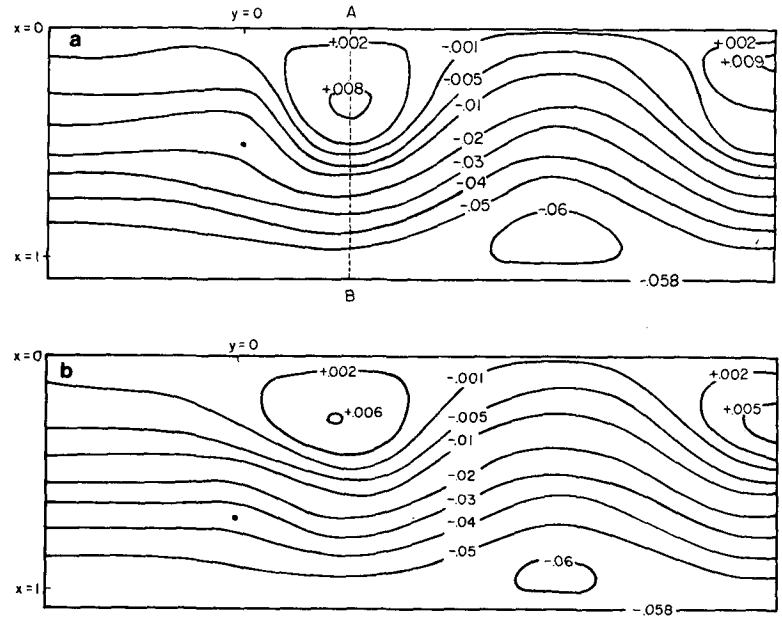

FIG. 6. Resultant streamline patterns for (a) case 2, $x_0 = 0.5$ and (b) case 2, $x_0 = 0.7$. The dimensionless volume of the bump (ϵV_b) is chosen to be 0.03.

flections near the coast are consistent with observations from satellite-borne infrared photography that billowlike undulations of the Gulf Stream frequently occur on its inshore side (Rhines, 1977). These large deflections can be understood as follows. Let x_0 be the upstream location of a streamline and $\eta = x - x_0$ be the deflection of a streamline. The equation of a streamline, i.e., $x_0 = f(x,y)$, can be determined from

$$\psi_0(x_0) = \psi_0(x) + \epsilon\psi(x,y) + O(\epsilon^2)$$

or

$$\psi_0(x - \eta) = \psi_0(x) + \epsilon\psi(x,y) + O(\epsilon^2).$$

For small η we can expand the left-hand side in a Taylor series

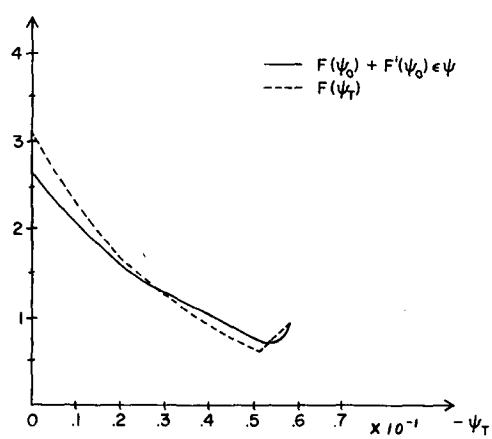

FIG. 7. $F(\psi_T)$ and $F(\psi_0) + F'(\psi_0)\epsilon\psi$ versus $|\psi_T|$ across section A–B of Fig. 6a.

$$\psi(x) - \eta\psi_{0x} + \tfrac{1}{2}\eta^2\psi_{0xx} = \psi_0(x) + \epsilon\psi(x,y) + O(\epsilon^2).$$

In general, $\eta = O(\epsilon)$ except near the coast where $\psi_{0x} \to 0$. In this region $\eta = O(\epsilon^{1/2})$. Orlanski's (1969) calculations with two-layer model also showed baroclinic waves near shore in the upper layers of the Florida Current which quite easily can be excited by a "bump".

In Fig. 6b, the topography and velocity field are the same as in Fig. 6a, but the singularity is located at $x_0 = 0.7$. As expected, streamline deflections are somewhat less because the amplitude of the wave is smaller. At first sight Figs. 6a and 6b do not seem to be small perturbed solutions. One may question whether our approximation [Eq. (5)] can still be valid for such a large-amplitude perturbation. To answer this problem, we compute $F(\psi_T)$ and the two-term Taylor's expansion of $F(\psi_T)$ along one of the worst cross sections in Fig. 6a (the cross section A–B). The results are shown in Fig. 7, which justifies our *a priori* assumption, i.e., the two-term Taylor's expansion is a good approximation of $F(\psi_T)$, even for a dimensionless volume of the bump as large as 0.03. Further, from the formulation in Section 2a, we also notice that the existence of the reversed flow in the eddy regions is allowable and does not upset our perturbation scheme.

The preceding two cases have α large so that $\psi(1,y) \approx 0$. Therefore, in Fig. 8 we choose $b = 0.5$, $c = 15.8$, $\theta = 1.31$ (case 4), and $x_0 = 0.7$, which has $\alpha = 3.03$ and $M = 106$ Sv. Comparing Figs. 6a with 6b we see that the wavelength is longer

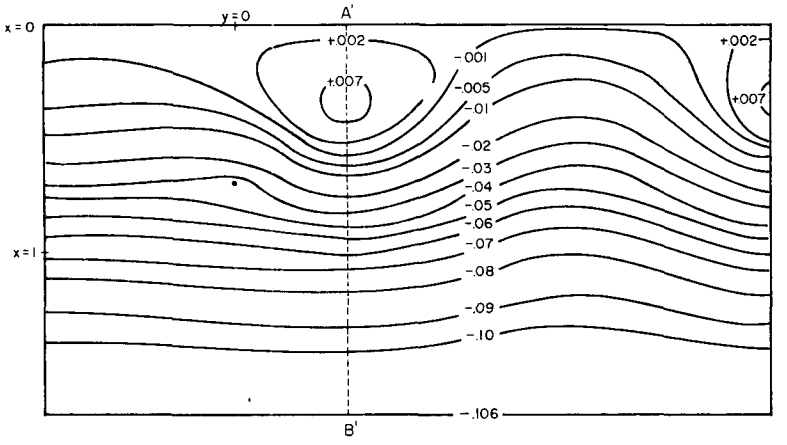

FIG. 8. Resultant streamline pattern for case 4, $x_0 = 0.5$. The dimensionless volume of the bump (ϵV_b) is chosen to be 0.03.

for M larger, a weak disturbance does extend beyond $x = 1$, and the weak offshore eddies disappear. We note that in all the above cases there is a decrease in velocity just upstream and slightly seaward of the topography, and there is some splitting of the stream as it passes over the topography. The velocity shear and bottom slope are not the cause of this phenomenon, since it is present in uniform flows over isolated topographic features as shown in the work of Vaziri and Boyer (1971). To justify our *a priori* assumption that the two-term Taylor's expansion is a valid approximation, we again compute $F(\psi_T)$ and $F(\psi_0) + F'(\psi_0)\epsilon\psi$ across one of the worst section (cross section A'–B') in Fig. 8. The result justifying that the approximation [Eq. (5)] is valid is shown in Fig. 9.

Our numerical work shows that 1) there is a seaward deflection of the current downstream of the singularity; 2) there are a series of lee waves and associated eddies on the inshore side of the stream; 3) if α is large there are offshore eddies one-half a wavelength downstream of the inshore eddies; 4) if α is large the rigid-wall approximation is valid and the results of Eqs. (40) and (41) may be applied; and 5) lee shelf waves near shore usually have larger amplitudes of deflection than those off shore.

4. Conclusions

This model was initially developed in an attempt to explain the seaward deflection and presence of waves and eddies downstream (north) of the Charleston bump. It is clear, given the nature of the topography in this region (i.e., the northward narrowing of the shelf region), that the model is at best qualitatively applicable to this region. However, the amplitude of the seaward deflection and the wavelengths generated are quite reasonable when compared to satellite imagery. A more realistic model of this region would include the narrowing shelf. This model may be applicable to other situations when a coastal jet flows over a more uniform continental margin. The result for large α is that the boundary condition $\psi(1,y) = 0$ may also be applicable to other problems.

We also notice that the approximation [Eq. (5)] works only for some special classes of sheared current profiles (in our case we assume $h\Pi_x/V$ = constant). For an arbitrarily chosen sheared current profile such that $V(x = 0) = 0$ and $h\Pi_x(x = 0) \neq 0$, the coastline ($x = 0$) is then a critical layer, which usually makes our Taylor's expansion [Eq. (5)] invalid. A more cumbersome analysis is then needed.

Although we consider only a Green's function solution by shrinking the size of the bump to zero and keeping the volume of the bump fixed in this paper, the result can easily be adapted to an extended topographic irregularity by intergrating the Green's function solution over the extended region.

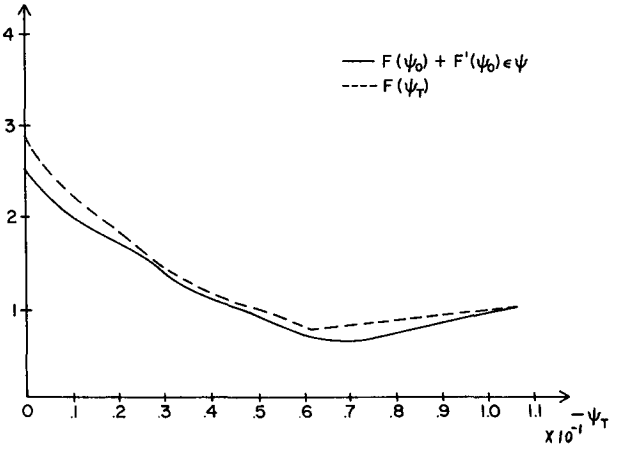

FIG. 9. $F(\psi_T)$ and $F(\psi_0) + F'(\psi_0)\epsilon\psi$ versus $|\psi_T|$ across section A'–B' of Fig. 8.

If we identify the Green's function solution for the perturbed streamfunction as ψ_G [i.e., Eqs. (32) and (33) for a delta-function bump placed at (x_0,y_0)] and let the topographic irregularity extend over a region of longshore scale l_y and cross-shelf scale l_x, the total perturbed streamfunction ψ is then

$$\psi(x,y) = \int_{l_y}\int_{l_x} \bar{h}(x_0,y_0)\psi_G(x,x_0;\, y,y_0)dx_0dy_0. \quad (42)$$

One can easily see from (32) and (33) that if $l_y \ll k_0^{-1}$ and $l_x \ll (\beta^2 - k_0^2)^{-1/2}$, then the Green's function solution is approximately valid for regions away from the bump. As l_x and l_y get larger, the oscillations of ψ_G in both the x and y directions when we perform the integration (42) must then be taken into consideration, and the Green's function solution gradually loses its meaning. However, for topographies which $l_y < \frac{1}{2}L$ the error involved in using a point simulation is less than 10% away from the singularity.

It has long been suggested that Gulf Stream meanders and eddies are important to the shelf water circulation off the Carolina coast. Abbe (1895) suggested that "back-set eddies" on the inshore side of the Gulf Stream were responsible for the formation of the cusplike Carolina coastal boundary. Mysak and Hamon (1969) found southward propagation of sea level disturbances in Onslow Bay. Based on the crude model we have developed, one might suspect that the Charleston bump is the possible cause. This suspicion is somewhat justified by the fact that the cuspate coastal boundary of the Carolinas appears only north of Charleston bump, and that the length of the bays is of the order of 150 km, comparable to the wavelength of lee waves downstream of Charleston. However, the above speculation is suggestive rather than conclusive.

Acknowledgment. The authors would like to express their thanks to Dr. L. J. Pietrafesa for suggesting, two years ago, that the Charleston bump might be responsible for the seaward deflection of the Gulf Stream, and to Dr. D. A. Brooks for his helpful discussions on shelf waves. The final draft of this paper was completed when one of the authors (SYC) was a contractor at NASA/Goddard Space Flight Center. The administrative help and helpful discussions he received from Drs. James Mueller, Richard Barbieri and Timonthy Kao are also acknowledged. This work was supported by the National Science Foundation under Grant ATM 76-15871.

REFERENCES

Abbe, C., Jr., 1895: Remarks on the cuspate capes of the Carolina coast. *Proc. Boston Soc. Nat. Hist.*, **26**, 489–497.

Brooks, D. A., 1976: Subtidal sea level fluctuations and their relation to atmospheric forcing along the North Carolina coast. *J. Phys. Oceanogr.*, **8**, 481–493.

Buchwald, V. T., and J. K. Adams, 1968: The propagation of continental shelf waves. *Proc. Roy. Soc. London*, **A305**, 235–250.

Cottrell, J. W., 1971: Is the Great Red Spot of Jupiter a Taylor column in horizontal shear flow? WHOI-GFD Summer School notes, Vol. 2, 15–32.

Hogg, N. G., 1973: On the stratified Taylor column. *J. Fluid Mech.*, **58**, 517–537.

Janowitz, G. S., 1975: The effect of bottom topography on a stratified flow in the beta plane. *J. Geophys. Res.*, **80**, 4163–4168.

Johnson, E. R., 1978: Quasigeostrophic flow above sloping boundaries. *Deep-Sea Res.* (in press).

Legeckis, R., 1978: A survey of worldwide sea surface temperature fronts detected by environmental satellites. *J. Geophys. Res.*, **83**, 4501–4524.

McCartney, M. S., 1975: Inertial Taylor columns on a beta-plane. *J. Fluid Mech.*, **68**, 71–95.

Mysak, L. A., and B. V. Hamon, 1969: Low-frequency sea level behavior continental shelf waves off North Carolina. *J. Geophys. Res.*, **74**, 1397–1405.

Niiler, P. P., and L. A. Mysak, 1971: Barotropic waves along an eastern continental shelf. *Geophys. Fluid Dyn.*, **2**, 273–288.

Orlanski, I., 1969: The influence of bottom topography on the stability of jets in a baroclinic fluid. *J. Atmos. Sci.*, **26**, 1216–1332.

Rhines, P. B., 1977: The dynamics of unsteady currents. *The Sea*, E. D. Goldberg, I. N. McCave, J. J. O'Brien and J. H. Steele, Eds., Vol. 6, Wiley-Interscience, 189–318.

Vaziri, A., and D. L. Boyer, 1971: Rotating flow over shallow topographies. *J. Fluid Mech.*, **50**, 79–96.